10382 *Macromolecules* **2010**, *43*, 10382–10389
DOI: 10.1021/ma1020159

Macromolecules
ARTICLE

Synthesis and Charge Transport Properties of Redox-Active Nitroxide Polyethers with Large Site Density

Kenichi Oyaizu, Takeshi Kawamoto, Takeo Suga, and Hiroyuki Nishide*

Department of Applied Chemistry, Waseda University, Tokyo 169-8555, Japan

Received August 31, 2010; Revised Manuscript Received November 16, 2010

ABSTRACT: To maximize the theoretical redox capacity of polymers containing cyclic nitroxides as redox-active pendant groups for high-density charge storage application, a compact five-membered ring with the smallest equivalent weight among the robust cyclic nitroxides was directly bound to a poly(ethylene oxide) chain. 2,2,5,5-Tetramethyl-3-oxiranyl-3-pyrrolin-1-oxyl was synthesized and polymerized via anionic coordinated ring-opening polymerization utilizing diethyl zinc/H_2O as an initiator. The unpaired electron in the monomer survived during the polymerization, giving rise to a high density redox polymer with a weight-specific theoretical capacity of 147 mA h/g. Cyclic voltammetry of the polymer layer confined at the surface of an electrode revealed a large redox capacity comparable to the theoretical capacity, which was ascribed to the efficient swelling and yet insoluble properties of the polyether in electrolyte solutions by virtue of the high molecular weight of $>10^5$ and adhesive properties allowing immobilization of the layer on the electrode surface. The redox capacity also indicated that the ionophoric polyether matrix accommodated electrolyte anions through the polymer/electrolyte interface to neutralize positive charges produced by the oxidation of the neutral radicals at the polymer/electrode interface. The diffusion coefficient for the redox gradient-driven charge hopping process corresponded to a large second-order rate constant in the order of 10^7 M^{-1} s^{-1}, which suggested an efficient electron self-exchange reaction throughout the polymer layer due to the large redox site population and hence to the small intersite distance. Test cells fabricated with a polymer/carbon fiber composite layer on an aluminum current collector as the cathode and a Li anode sandwiching an electrolyte layer were capable of charging and discharging as a secondary battery with an output voltage near 3.7 V and were durable for more than 10^3 charging−discharging cycles without substantial degradation.

Introduction

Polymers containing organic robust radical groups,[1] such as NO-centered nitroxides and nitronyl nitroxides, N-centered triarylaminium cation radicals, and O-centered phenoxyls and galvinoxyls, are an interesting class of materials in which the presence of the unpaired electron can lead to unusual electronic,[2] magnetic,[3] and optical properties.[4] Broad attention has been given especially to nonconjugated polymers bearing cyclic nitroxides such as 2,2,6,6-tetramethylpiperidin-1-oxyl (TEMPO) and 2,2,5,5-tetramethyl-1-pyrrolidineoxy (PROXYL)[5] due to the opportunity to reversibly switch between the oxidation states of the neutral radical $\rangle N-O\cdot$ and the oxoammonium cation $\rangle N^+{=}O$ combined with the exceptionally high stability of both redox states under ambient conditions.[6] These so-called "radical polymers" also constitute an extensively studied group of functional polymers for charge transport and storage.[7] A recent example that typically illustrates this concept is our approach to the "radical battery" which is characterized by an excellent rate performance and capability of fabricating purely organic, flexible, paperlike, and transparent rechargeable energy-storage devices.[8] Our principal finding is that the radical polymer layers, immobilized on electrodes and swollen in electrolyte solutions, exhibit substantial redox capacity, which indicates that the mass-transfer process for electrolyte ions is accomplished to neutralize charges produced by the electrode reaction.[9] Poly(1-oxy-2,2,6,6-tetramethylpiperidin-4-yl methacrylate) (PTMA)[10] and poly(1-oxy-2,2,6,6-tetramethylpiperidin-4-yl vinyl ether) (PTVE)[11] have been the most typically employed as the cathode-active materials. However, the energy density of the fabricated device has been limited by the intrinsic redox capacity of the radical polymers. Indeed, the calculated weight-specific capacities of PTMA (112 mA h/g) and PTVE (135 mA h/g) are smaller than the conventional cathode-active materials in Li ion batteries such as $LiCoO_2$ ($\geq$137 mA h/g for $LiCoO_2 = xLi^+ + Li_{1-x}CoO_2 + xe^-$ and $x \geq 0.5$). To increase the theoretical redox capacity of the radical polymer by reducing the formula weight per repeating unit, while maintaining the affinity to electrolyte solutions, is an important subject of the current research.

We previously found that poly(1-oxy-2,2,6,6-tetramethylpiperidin-4-yl glycidyl ether) (PTGE) was an excellent cathode-active material and reported that the efficient charge transport/storage property was attributed to the flexible and ionophoric poly(ethylene oxide) (PEO) backbone to allow propagation of charges deeply into the polymer layer from the polymer/electrode interface.[12] In here, we design and synthesize a polymer **1** (Figure 1) in which the 2,2,5,5-tetramethyl-3-pyrrolin-1-oxyl group with the smallest equivalent weight among the robust cyclic nitroxides is directly bound to the PEO chain per repeating unit. We focus on the large weight-specific capacity of 147 mA h/g derived from the compact unit and a dramatically facilitated charge hopping process in the polymer layer as a result of the small intersite distance δ_{av} (Figure 1), which offered insights into the kinetic aspects of an electron self-exchange reaction and a strategy to further improve the capacity and the rate performance of the radical battery.

Experimental Section

Materials. All solvents were purified by distillation prior to use. A vapor-grown carbon fiber (VGCF) was obtained from

*Corresponding author: Tel +81-3-3200-2669; Fax +81-3-3209-5522; e-mail nishide@waseda.jp.

 Published on Web 12/02/2010

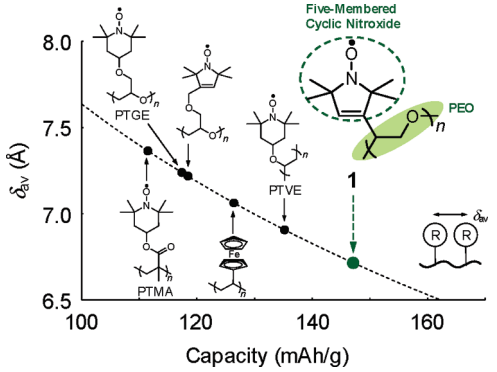

Figure 1. Plots of mean intersite distance δ_{av} versus redox capacities for polyethers and a poly(vinyl ether) bearing TEMPO or 2,2,5,5-tetramethyl-3-pyrrolin-1-oxyl groups as redox sites (R), together with those for poly(vinylferrocene) and PTMA. Dotted curve represents the mean intersite distance calculated from the formula weight per repeating unit, *fw*, according to $\delta_{av} = (fw/N_A)^{1/3} = N_A^{-1/3}(1000F/3600)^{1/3}(\text{capacity})^{-1/3}$, assuming a molecular density of 1 g/cm^3.

Scheme 1. Synthesis of the Polyether 1

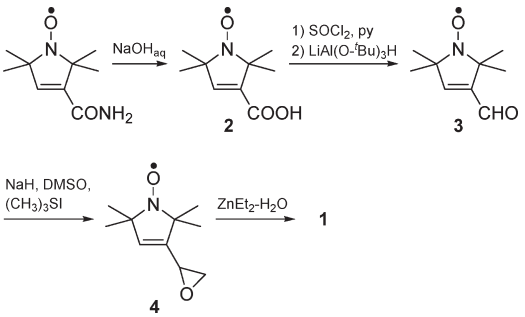

Showa Denko Co. A binder powder, poly(vinylidene fluoride) (PVdF) resin (KF polymer), was purchased from Kureha Chemical Co. Tetrabutylammonium perchlorate ($TBAClO_4$) was obtained from Tokyo Kasei Co. and purified by recrystallization. An electrochemical grade solution of 1 M lithium hexafluorophosphate ($LiPF_6$) in ethylene carbonate/diethyl carbonate (1/1 in v/v) was obtained from Kishida Kagaku Co. A 1 M solution of potassium *tert*-butoxide (*t*-BuOK) in THF was obtained from Aldrich Co. All other regents were obtained from Kanto Chemical Co. or Tokyo Kasei Co. and were used without further purification.

Synthesis of Epoxide Monomer. The oxiranyl group in **4** was derived in three steps from a carbamoyl group according to Scheme 1. The paramagnetic products were characterized by NMR spectroscopy after conversion to the corresponding diamagnetic *N*-hydroxy-2,5-dihydropyrrole derivatives using phenylhydrazine as a reducing agent.

3-Carboxy-2,2,5,5-tetramethyl-3-pyrrolin-1-oxyl (2). 3-Carbamoyl-2,2,5,5-tetramethyl-3-pyrrolin-1-oxyl (0.011 mol, 2.03 g) was added to a 10 wt % aqueous NaOH solution (28.8 mL, 0.072 mol), which was refluxed for 2 h until the generation of the eliminated NH_3, monitored using a flow meter, was finished. The resulting yellow solution was neutralized with 10 mol % HCl. Extraction of the product with diethyl ether and recrystallization from diethyl ether/hexane yielded **2** as a yellow crystal. Yield: 1.30 g (7.1 mmol, 64%). FAB-MS (*m*/*z*): calcd for M^+ 184.21; found 186, 183. IR (KBr, cm^{-1}): 1717 ($\nu_{C=O}$). Anal. Calcd for $C_9H_{14}NO_3$: C, 58.68; H, 7.66; N, 7.60%. Found: C, 57.92; H, 7.54; N, 7.50%. ^{1}H NMR ($CDCl_3$, 600 MHz, ppm, TMS, after reduction with phenylhydrazine): δ 7.23 (s, 1H), 6.49 (s, 1H), 1.56 (s, 6H), 1.46 (s, 6H). ^{13}C NMR ($CDCl_3$, 150 MHz, ppm, TMS, after reduction with phenylhydrazine): δ 169.0, 140.5, 137.7, 76.1, 72.6, 23.5, 23.2, 22.8, 22.5.

3-Formyl-2,2,5,5-tetramethyl-3-pyrrolin-1-oxyl (3). The carboxylic acid **2** (1.26 g, 6.84 mmol) was dissolved in a mixture of benzene (15 mL) and pyridine (0.55 mL, 6.84 mmol). The resulting solution was maintained at 5−8 °C using ice bath, to which was added a solution of thionyl chloride (0.55 mL, 7.74 mmol) in benzene (2.3 mL). After stirring for 1 h and removal of the solvent by rotary evaporation, the product was dissolved in dehydrated THF (12.5 mL) under argon. To this solution was added a solution of lithium aluminum *tert*-butoxide hydride (LiAl(O-^{t}Bu)$_3$H) (1 M) in THF (6.79 mL, 6.79 mmol, 1 equiv) at −78 °C under argon, which was kept stirring for 2 h under the reduced temperature. (Note that addition of excess LiAl-(O-^{t}Bu)$_3$H led to a lower product yield as a result of the side reaction to give 3-hydroxymethyl-2,2,5,5-tetramethyl-3-pyrrolin-1-oxyl.) After removal of the solvent by rotary evaporation, the product was extracted with ethyl acetate and purified by silica gel column chromatography using diethyl ether/hexane (7/3 in v/v) as an eluent to give **3** as a yellow crystal. Yield: 0.72 g (42.8 mmol, 62%). FAB-MS (*m*/*z*): calcd for M^+ 168.21; found 168. IR (KBr, cm^{-1}): 1684 ($\nu_{C=O}$). Anal. Calcd for $C_9H_{14}NO_2$: C, 64.26; H, 8.39; N, 8.33%. Found: C, 63.78; H, 8.64; N, 8.16%. ^{1}H NMR ($CDCl_3$, 600 MHz, ppm, TMS, after reduction with phenylhydrazine): δ 9.62 (s, 1H), 6.43 (s, 1H), 1.38 (s, 6H), 1.33 (s, 6H). ^{13}C NMR ($CDCl_3$, 150 MHz, ppm, TMS, after reduction with phenylhydrazine): δ 188.7, 146.0, 144.4, 68.8, 68.4, 25.2, 24.8, 24.6, 24.3.

Scheme 2. Synthesis of the 3-Oxiranyl PROXYL 8

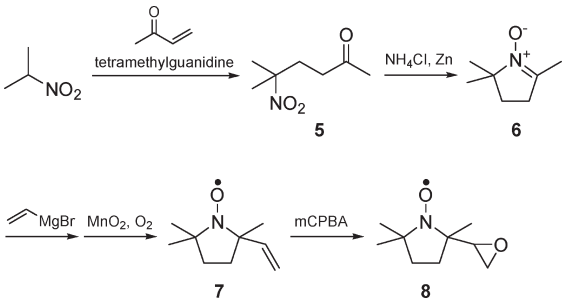

2,2,5,5-Tetramethyl-3-oxiranyl-3-pyrrolin-1-oxyl (4). Sodium hydride (211 mg) was added to DMSO (3.18 mL) under argon and reacted for 1 h at 65 °C. The mixture was diluted with THF (4.0 mL). The solution was cooled to −10 °C using ice bath with $CaCl_2$, to which was added a solution of trimethylsulfonium iodide (1.03 g) in DMSO (4.00 mL) and stirred for 5 min under argon. A solution of **3** (703 mg) in THF (1.6 mL) was slowly added to the solution, which was kept stirring for 30 min at −10 °C and for 2 h at room temperature. Extraction with ethyl acetate and purification by column chromatography using ethyl acetate/hexane (1/1 in v/v) as an eluent (R_f = 0.64) followed by HPLC with $CHCl_3$ yielded the epoxide monomer **4** as an orange liquid. Yield: 0.53 g (70%). FAB-MS (*m*/*z*): calcd for M^+ 182.24; found 182. IR (KBr, cm^{-1}): 1249 (ν, epoxide 8 μ), 932 (ν, epoxide 11 μ), 772 (ν, epoxide 12 μ). Anal. Calcd for $C_{10}H_{16}NO_2$: C, 65.91; H, 8.85; N, 7.69%. Found: C, 65.18; H, 8.80; N, 8.36%. The radical concentration was determined to be 100% by comparing the ESR intensity with that of 3-carbamoyl-2,2,5,5-tetramethyl-3-pyrrolin-1-oxyl. ^{1}H NMR ($CDCl_3$, 600 MHz, ppm, TMS, after reduction with phenylhydrazine): δ 6.83 (s, 1H), 3.28 (t, 1H), 2.78 (d, 2H), 1.34 (s, 3H), 1.30 (s, 3H), 1.23 (s, 3H), 1.21 (s, 3H). ^{13}C NMR ($CDCl_3$, 150 MHz, ppm, TMS, after reduction with phenylhydrazine): δ 151.3, 119.5, 70.4, 68.1, 49.4, 47.7, 26.1, 25.6, 25.4, 24.8.

Synthesis of Oxiranyl-Substituted PROXYL. 2,5,5-Trimethyl-3-oxiranyl-pyrrolidinoxyl (**8**) was synthesized according to Scheme 2, as an alternative epoxide designed to give the radical polyether.

5-Nitrohexane-2-one (5). Methyl vinyl ketone (0.509 mol, 35.7 g) was dissolved in CH_3CN (130 mL). After addition of 2-nitropropane (0.56 mol, 50 g) to the solution, tetramethylguanidine (50.9 mmol, 5.86 g) was added dropwise at 0 °C. The resulting mixture was stirred for 24 h at room temperature. After addition of

aqueous HCl, the product was extracted with diethyl ether, washed with H_2O, and purified by distillation under reduced pressure to yield **5** as a colorless liquid. Yield: 32%. FAB-MS (*m*/*z*): calcd for M^+ 159.18; found 159. IR (KBr, cm^{-1}): 1719, 1348. Anal. Calcd for $C_7H_{13}NO_3$: C, 52.82; H, 8.23; N, 8.80%. Found: C, 52.60; H, 8.41; N, 8.81%. ^{1}H NMR ($CDCl_3$, 600 MHz, ppm, TMS): δ 2.45 (t, 2H), 2.19 (t, 2H), 2.16 (s, 3H), 1.58 (s, 6H). ^{13}C NMR ($CDCl_3$, 150 MHz, ppm, TMS): δ 206.3, 87.3, 38.1, 33.9, 29.9, 25.8.

2,2,5-Trimethyl-3,4-dihydro-2*H*-pyrrole 1-Oxide (6). To the nitroketone **5** (5.1 g) was added an aqueous solution of ammonium chloride. After cooling to 0 °C, a zinc powder was slowly added to the solution which was kept stirring for 1 h at 0 °C and then for 2 h at room temperature. Removal of zinc by filtration, washing with CH_3OH, extraction with CH_3Cl, and distillation under reduced pressure gave **6** as a colorless liquid. Yield: 1.7 g. FAB-MS (*m*/*z*): calcd for M^+ 127.18; found 127. IR (KBr, cm^{-1}): 1627 ($\nu_{C=N}$). ^{1}H NMR ($CDCl_3$, 600 MHz, ppm, TMS): δ 2.59 (t, 2H), 2.03 (s, 3H), 2.00 (t, 2H), 1.40 (s, 6H). ^{13}C NMR ($CDCl_3$, 150 MHz, ppm, TMS): δ 141.9, 100.5, 73.1, 32.2, 29.1, 25.3, 13.0.

2,2,5-Trimethyl-5-vinylpyrrolidinoxyl (7). To a solution of **6** (1.80 g) in THF (17 mL) was added a 1 M solution of vinylmagnesium bromide in THF (17.4 mL) under argon, which was kept stirring for 2 h at room temperature. After evaporating the solvent, extraction of the product with diethyl ether followed by purification by silica gel column chromatography using hexane/ethyl acetate (10/1 in v/v) as an eluent yielded **7** as an orange liquid. Yield: 0.5 g. FAB-MS (*m*/*z*): calcd for M^+ 154.2; found 154. IR (KBr, cm^{-1}): 3087 (ν_{C-H}), 1639 ($\nu_{C=C}$). ^{1}H NMR ($CDCl_3$, 600 MHz, ppm, TMS): δ 6.18 (t, 1H), 5.10 (d, 2H), 1.93 (m, 1H), 1.73 (m, 3H), 1.33 (s, 3H), 1.24 (s, 3H), 1.17 (s, 3H). ^{13}C NMR ($CDCl_3$, 150 MHz, ppm, TMS): δ 152.6, 145.5, 65.7, 61.8, 34.5, 32.4, 26.7, 26.1, 24.5.

2,5,5-Trimethyl-3-oxiranylpyrrolidinoxyl (8). To **7** (100 mg) was added a solution of *m*-chloroperbenzoic acid (mCPBA) (121.8 mg) in CH_2Cl_2 (10 mL). The resulting solution was stirred for 15 min at 0 °C and then for 12 h at room temperature. Extraction of the product with diethyl ether followed by purification by slica gel column chromatography using hexane/diethyl ether (2/1 in v/v) yielded the *RS*-mixture of the monomer **8** as an orange liquid. Yield: 40 mg. FAB-MS (*m*/*z*): calcd for M^+ 170.1; found 170. IR (KBr, cm^{-1}): 1255 (ν, epoxide 8 μ), 911 (ν, epoxide 11 μ), 865 (ν, epoxide 12 μ). ^{1}H NMR ($CDCl_3$, 600 MHz, ppm, TMS, after reduction with phenylhydrazine): δ 3.04 (t, 1H), 2.69 (m, 2H), 1.70−1.50 (m, 4H), 1.25 (s, 3H), 1.17 (s, 3H), 1.15 (s, 3H). ^{13}C NMR ($CDCl_3$, 150 MHz, ppm, TMS, after reduction with phenylhydrazine): δ 57.0, 44.2, 38.2, 34.6, 29.8, 27.1, 25.9, 22.9, 21.1.

Anionic Coordinated Ring-Opening Polymerization of 4. A 1 M hexane solution of diethylzinc was cooled to −78 °C, to which was added H_2O (1 equiv) under argon. The mixture was slowly heated to room temperature and stirred for 1 h to give the yellow solution of the $ZnEt_2/H_2O$ initiator. To the monomer **4** was added the initiator (10 mol %) under strictly anaerobic conditions. The mixture was stirred at 40 °C for 24 h (entry 5 in Table S1), which gelated during the reaction. The resulting mixture was dissolved in THF and slowly poured into hexane. The precipitate was collected by filtration, which was dissolved in THF. The residual zinc catalyst was insoluble in THF, which was removed by centrifugation. The polymer was purified by reprecipitation from diethyl ether to yield a yellow powder. Yield: 6 wt % (entry 5 in Table S1). The obtained polymer was partially soluble in THF and $CHCl_3$ but insoluble in CH_3CN and propylene carbonate. GPC (THF, polystyrene standard): $M_n = 1.2 \times 10^5$, $M_w = 3.5 \times 10^5$. IR (KBr, cm^{-1}): 1042 (ν_{C-O-C}). Anal. Calcd for $C_{10}H_{16}NO_2$: C, 65.91; H, 8.85; N, 7.69%. Found: C, 65.20; H, 8.80; N, 8.40%. ^{1}H NMR ($CDCl_3$, 600 MHz, ppm, TMS, after reduction with phenylhydrazine): δ 5.58 (s, 1H), 3.29 (d, 2H), 2.60 (t, 1H), 1.26 (s, 12H). ^{13}C NMR ($CDCl_3$, 150 MHz, ppm, TMS, after reduction with phenylhydrazine): δ 141, 132, 70.6, 68.1, 49.2, 47.4, 25.1. DSC (10 °C/min, under argon): T_g = 44 °C. TG-DTA (10 °C/min, under argon): $T_{d10\%}$ (temperature for 10% weight loss) = 192 °C.

Anionic Ring-Opening Polymerization of 4. To a solution of **4** in THF was added a solution of *t*-BuOK in THF (10 mol %) under argon (entry 8 in Table S1). The mixture was stirred at 60 °C for 24 h. The resulting mixture was dissolved in $CHCl_3$ and slowly poured into hexane. The precipitate was collected by filtration, dissolved again in THF, and purified by reprecipitation from hexane and dried under vacuum at room temperature to yield the oligomer as an yellow powder. Yield: 20 wt %. GPC (THF, polystyrene standard): $M_n = 8.4 \times 10^2$, $M_w = 9.2 \times 10^2$. IR (KBr, cm^{-1}): 1041 (ν_{C-O-C}).

Determination of the Radical Content. The polymer **1** (entry 5 in Table S1) was characterized by the *g*-value (2.0065) of the ESR signal, which was close to that of the monomer **4** at 2.0059. The radical concentrations were determined, assuming that the polymers were paramagnetic at room temperature, by comparing the integrated ESR intensity with that of the solution of **4** as the standard. A dual sample cavity was employed to allow accurate ESR integrations. The radical concentration was also determined by means of SQUID measurements using the Curie plots and the values for saturated magnetization. The two independently determined values agreed well with each other.

Preparation of 1/Carbon Composite Electrodes. The polymer **1** (entry 5 in Table S1, 5.0 mg) was mixed with VGCF (40.0 mg) and PVdF (5.0 mg) in *N*-methyl-2-pyrrolidone (NMP). The mixture was pasted on the aluminum foil (ca. 1.13 cm^2) and dried under vacuum at 40 °C for 10 h to give the composite electrode with a composition of **1**/VGCF/PVdF = 1/8/1 (w/w/w).

Electrochemical Measurements. Electrochemical analyses were carried out in a conventional cell under argon. The auxiliary electrode was a coiled platinum wire. The reference electrode was a commercial Ag/AgCl immersed in a solution of 0.1 M $TBAClO_4$ in CH_3CN. The formal potential of the ferrocene/ferrocenium couple was 0.45 V vs this Ag/AgCl electrode. An ALS 660B electrochemical analyzer was employed to obtain the voltammograms. Heterogeneous electron-transfer rate constants k_0 for the electrode reactions were determined from the variations of a peak-to-peak separation ΔE_p with a potential sweep rate v in cyclic voltammetry according to $k_0 = \psi\{\pi DFv/(RT)\}^{1/2}$ (Nicholson's method), where D was the diffusion coefficient of the reactant determined from the slope of the peak current−$v^{1/2}$ plot[13a] and ψ was given by the data linking to ΔE_p.[13b] The macroscopic diameter of the platinum disk microelectrode used for the electrochemical measurements (ϕ = 1.0 mm) was confirmed from the magnitude of the current for the electrolysis of ferrocene as the internal standard.

Fabrication and Characterization of Test Cells. A coin cell was fabricated by sandwiching the electrolyte layer of 1 M $LiPF_6$ in ethylene carbonate/diethyl carbonate (1/1 in v/v) with the **1**/carbon composite cathode and the Li anode, using the separator film (cell guard #2400 from Hohsen Co.) under anaerobic conditions. The cyclic performance of the fabricated cell was examined by repeated charging−discharging galvanostatic cycles at different current densities. The charging−discharging experiments were typically performed at a current density of 10 C, where 1 C represents the current density required for charging or discharging of the cell at 1 h.

Measurements. ^{1}H and ^{13}C NMR spectra were recorded on a JEOL JNM-LA500 or Bruker AVANCE 600 spectrometer with chemical shifts downfield from tetramethylsilane as the internal standard. Infrared spectra were obtained using a Jasco FT-IR 410 spectrometer with potassium bromide pellets. Molecular weight measurements were done by gel permeation chromatography using a TOSOH HLC8220 instrument with $CHCl_3$ as the eluent. Calibration was done with polystyrene standards. Elemental analyses were performed using a Perkin-Elmer PE-2400 II and a Metrohm 645 multi-DOSIMAT. Two parallel analyses were performed for each sample. Mass spectra were obtained using a JMS-SX102A or Shimadzu GCMS-QP5050 spectrometer. ESR spectra were recorded using a JEOL JES-TE200 spectrometer with a 100 kHz field modulation frequency and a 0.1 mT width. The magnetization and the magnetic susceptibility of

the powdery polymer samples were measured by a Quantum Design MPMS-7 SQUID magnetometer. The magnetic susceptibility was measured from 1.95 to 270 K in a 0.5 T field. Thermal analyses were performed by a Seiko DSC220C and TG/DTA 220 thermal analyzer under nitrogen.

X-ray Crystallography. All diffraction measurements were made on a Rigaku RAXIS RAPID imaging plate area detector with a graphite-monochromated Mo Kα radiation ($\lambda = 0.710\,75$ Å). The data were collected at 298 K. Crystal data for 3-carbamoyl-2,2,5,5-tetramethyl-3-pyrrolin-1-oxyl: $C_9H_{15}N_2O_2$, $M = 183.23$, orthorhombic space group $Pca2_1$ (No. 29), $a = 14.1743(7)$ Å, $b = 8.4983(4)$ Å, $c = 16.3600(8)$ Å, $V = 1970.68(17)$ Å^3, $Z = 8$, $D_{calcd} = 1.235$ g/cm^3, μ(Mo Kα) = 0.880 cm^{-1}. Of the 18 110 reflections, 4498 were unique ($R_{int} = 0.030$). The non-hydrogen atoms were refined anisotropically. Hydrogen atoms were refined isotropically. The final cycle of the full-matrix least-squares refinement was based on 3998 reflections with $I > 2\sigma(I)$ and 266 variable parameters and converged with $R = \sum||F_0| - |F_c||/\sum|F_0| = 0.0787$ and $R_w = (\sum w(F_0^2 - F_c^2)^2/\sum w(F_0^2)^2)^{1/2} = 0.2138$. Atomic coordinates, thermal displacement parameters, bond lengths and angles, and torsion angles are shown in Tables S2−S9. Crystal data for 3-carbamoyl-2,2,5,5-tetramethyl-1-oxo-2,5-dihydro-1*H*-pyrrolium hexafluorophosphate: $C_9H_{15}F_6N_2O_2P$, $M = 328.19$, triclinic space group $P\bar{1}$ (No. 2), $a = 8.402(6)$ Å, $b = 12.432(8)$ Å, $c = 14.584(9)$ Å, $\alpha = 69.184(16)°$, $\beta = 84.735(19)°$, $\gamma = 85.620(16)°$, $V = 1416.4(15)$ Å^3, $Z = 4$, $D_{calcd} = 1.539$ g/cm^3, μ(Mo Kα) = 2.641 cm^{-1}. Of the 13 196 reflections, 6332 were unique ($R_{int} = 0.078$). The non-hydrogen atoms were refined anisotropically. Hydrogen atoms were refined isotropically. The final cycle of the full-matrix least-squares refinement was based on 2829 reflections with $I > 2\sigma(I)$ and 391 variable parameters and converged with $R = \sum||F_0| - |F_c||/\sum|F_0| = 0.1282$ and $R_w = (\sum w(F_0^2 - F_c^2)^2/\sum w(F_0^2)^2)^{1/2} = 0.3286$. Atomic coordinates, thermal displacement parameters, bond lengths and angles, and torsion angles are shown in Tables S10−S17.

Results and Discussion

The 3-oxiranyl group in **4** was derived from the carbamoyl group by the hydrolysis into the carboxyl group in **2**, followed by the reduction to the formyl group in **3** via the carbonyl chloride, and epoxidation by the reaction of the resulting α,β-unsaturated ketone with dimethylsulfonium methylide $(CH_3)_2S{=}CH_2$ (Scheme 1).[14] A similar process to synthesize 2,2,5,5-tetramethyl-3-oxiranyl-1-pyrrolidineoxy (3-oxiranyl PROXYL) was unsuccessful due to the failure in the reduction step which produced the corresponding alcohol rather than the desired aldehyde, demonstrating that the partially reduced formyl group in **3** was significantly stabilized by the conjugation with the double bond in the ring. The oxiranyl-substituted PROXYL **8** was synthesized by the introduction of vinyl group to the 2,2,5-trimethyl-3,4-dihydro-2*H*-pyrrole 1-oxide **6** by the Grignard reaction followed by the oxidation with mCPBA (Scheme 2).

Cyclic voltammetry of **4** and **8** both revealed a reversible electrochemical response, which was ascribed to the oxidation of the nitroxide radicals to the corresponding oxoammonium cations $\mathbf{4}^+$ and $\mathbf{8}^+$, respectively. The cyclic voltammogram obtained for **4** at various scan rates revealed a totally reversible wave at $(E_{pa} + E_{pc})/2 = 0.87$ V vs Ag/AgCl, where E_{pa} and E_{pc} were the oxidation and the reduction peak potentials, respectively (Figure S1). The anodic and cathodic peak currents were equal and increased proportionally with the square root of the potential scan rate, which suggested that the electrode reaction was diffusion-limited and that both of the oxidized and reduced states were stable in the electrolyte solution. The peak-to-peak separation of $\Delta E_p = E_{pa} - E_{pc} = 60$ mV at small scan rates was close to the theoretical value of 59 mV. The electrolytic in-situ ESR spectroscopy revealed a hyperfine structure for **4** resulting from the nitrogen-centered ($I = 1$) radical (inset in Figure S1), which disappeared upon the anodic oxidation to $\mathbf{4}^+$. The heterogeneous electron-transfer rate constant k_0 was estimated by Nicholson's method,[13] based on the increase in ΔE_p at very large scan rates (> 1000 mV/s) with carefully compensated electrolyte resistance, which was accomplished by the combination of positive feedback circuitry and digital simulation methods. The rate constants for the $\mathbf{4}/\mathbf{4}^+$ and $\mathbf{8}/\mathbf{8}^+$ couples were 2.5×10^{-2} cm/s (Figure S1) and 1.0×10^{-1} cm/s, respectively, which were slightly smaller than or comparable to that for the TEMPO/TEMPO$^+$ couple (8.4×10^{-1} cm/s)[6b] and provided support for the proposed electrochemically reversible nature of the five-membered cyclic nitroxide. The rapid electron transfer with electrodes is advantageous for use as redox catalysts and electroactive materials because one could expect a large exchange current density of $j_0 = k_0FC^* > 10^0$ A/cm^2, which is desirable for battery applications,[15] by virtue of the large activity product C^* of the reactants or the redox site concentration (ca. 5 M) in the layer of **1**.

The rapid electron transfer process of **4** with electrodes originated from the relatively small structural changes accompanied by the redox reaction, which was demonstrated by the comparison of the crystal structures for 3-carbamoyl-2,2,5,5-tetramethyl-3-pyrrolin-1-oxyl and its oxidized product, 3-carbamoyl-2,2,5,5-tetramethyl-1-oxo-2,5-dihydro-1*H*-pyrrolium hexafluorophosphate (Figure 2). The chemical oxidation of the nitroxide was accomplished by the aerobic oxidation in the presence of HPF_6 to give bright yellow crystals of the oxoammonium salt. Single crystals were grown from methanol solutions. The atomic arrangement around the N1 atom revealed the electronic state of the N−O redox center. The N−O bond in the nitroxide shrank upon the oxidation to the oxoammonium cation by ca. 0.08 Å, as a result of an increased bond order. The small displacement of the oxoammonium nitrogen from the C_2O plane (Figure 2b) demonstrated the sp^2 character of the N1 atom. The nitroxide radical was characterized by moderate delocalization of the unpaired electron over the N−O center, resulting in a partial π-bond character of the N−O bond. The N1 atom in the radical was slightly displaced from the C_2O plane by 0.037 Å, which was intermediate between the sp^3 amines (0.58 Å) and the oxoammonium cation (0.01 Å) and was indicative of the partial sp^2 character. Organic molecules usually experience a large rearrangement of structural framework during the redox reactions through the bond scission and formation that must overcome activation energies. An account for the rapid electrode reaction observed for **4** is given by the relatively small atomic rearrangement required for the overall redox reaction to decrease the activation energy, in addition to the flexibility of the molecular framework and the stability of the radical.

The anionic coordinated ring-opening polymerization of **4** initiated with the $ZnEt_2/H_2O$ catalyst yielded the polymer **1** (entries 1−7 in Table S1). The product was partially soluble in $CHCl_3$ and THF and insoluble in other common organic solvents but swollen in the electrolyte solution employed for the electrochemical measurements. The swelling but insoluble property of the polymer was favorable for battery applications to impede a self-discharge accompanied by the undesired dissolution into the electrolyte solutions and was likely to be ascribed to the high molecular weight of $M_n \sim 1 \times 10^5$, which was suggested from the GPC analysis for the $CHCl_3$-soluble fraction of the product.

The anionic ring-opening polymerization of **4** using *t*-BuOK as the initiator produced oligomers with low unpaired electron densities. The similar incompatibility of the monomer with the five-membered cyclic nitroxide group has been observed for the polymerization of 2,2,5,5-tetramethyl-3-oxiranylmethoxymethyl-2,5-dihydro-1*H*-pyrrol-1-oxyl.[12a] Even more difficulty was found for the polymerization of **8** (entries 11 and 12 in Table S1). Other initiators reported for the anionic coordinated ring-opening polymerization, such as aluminum complexes,[16] were not effective

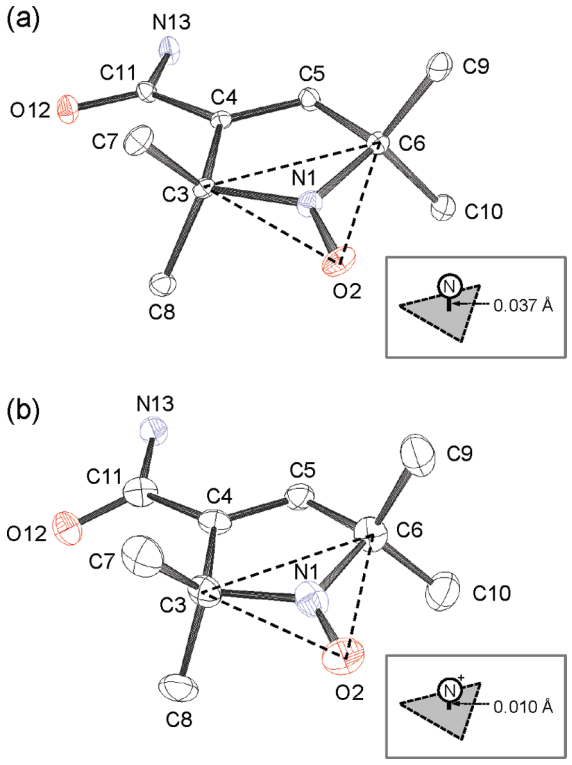

Figure 2. ORTEP drawing (50% probability ellipsoids) for 3-carbamoyl-2,2,5,5-tetramethyl-3-pyrrolin-1-oxyl (a) and 3-carbamoyl-2,2,5,5-tetramethyl-1-oxo-2,5-dihydro-1*H*-pyrrolium hexafluorophosphate (b), showing the deviation of N1 from O2−C3−C6 planes. Crystals of the radical (a) and the cation (b) both contained crystallographically independent molecules in the unit cell (not shown). The anion in (b) was omitted for clarity. Mean bond lengths (Å) for N1−O2: (a) 1.267, (b) 1.187.

for the polymerization of **8**, which reacted rather with the radical groups to undergo decomposition.

Reasoning that polymerization of **8** might have been sterically impeded by the bulky ring adjacent to the epoxide, we turned to focus on the polymerization of **4** to obtain the product with a high unpaired electron density by optimizing the reaction conditions. We found that the $ZnEt_2/H_2O$-initiated polymerization of **4** at a monomer/initiator ratio of $[M]_0/[I]_0 = 10$ under bulk conditions maintained at 40 °C yielded **1** possessing an unpaired electron per repeating unit (entry 5 in Table S1). Magnetic measurements revealed that the unpaired electron in the monomer survived during the polymerization, giving rise to the unpaired electron density of 100% (i.e., 1.0 spin/repeating unit) (vide infra). The structure-defined and high-molecular-weight radical polyether with a high radical site density was first obtained by the present method. Polymerization at elevated or reduced temperatures and at different $[M]_0/[I]_0$ ratio yielded the products in lower molecular weights and/or unpaired electron densities, which suggested that undefined parallel reactions coincided during the polymerization.

Thermal analysis revealed that the decomposition of **1** was initiated at temperatures higher than 170 °C and became significant around 180 °C, but 90 wt % of the polymer remained up to $T_{d10\%} = 192$ °C. The thermal stability against the 10% weight loss was lower than that of PTMA ($T_{d10\%} = 263$ °C).[10a] The slow decomposition initiated below 190 °C is characteristic of the polyether backbone and could be ascribed to the abstraction of hydrogen adjacent to the polyether oxygen atom by the nitroxide radical.[12a] The cyclic nitroxide group on the polyether backbone was stable at temperatures below 190 °C without substantial decomposition until the thermolysis of the backbone was initiated, which was confirmed by monitoring the unpaired electron

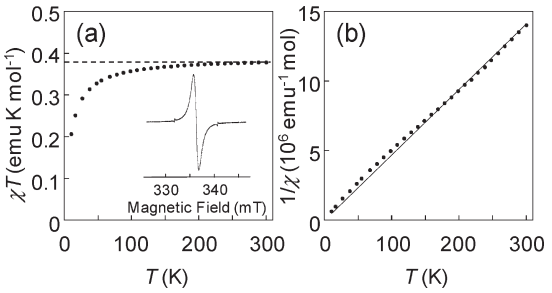

Figure 3. $\chi_{mol}T$ vs T (a) and $1/\chi_{mol}$ vs T plots with the Curie−Weiss fitting (solid line) (b) for **1** (11.0 mg) obtained by SQUID measurements, where χ_{mol} is based on per mole of the nitroxide radical. Dashed line in (a) represents the theoretical value of $\chi_{mol}T$ for $S = {}^1/_2$. Inset in (a) shows ESR spectrum obtained for the solution of **1** (2.00 mmol unit/L) in CH_2Cl_2 at room temperature. Small signals near 332 and 340 mT in the ESR spectrum are from the Mn^{2+}/MgO standard.

density by the SQUID measurement. The polyether backbone was characterized by the low glass transition temperature (T_g = 44 °C). The increased flexibility, compared with PTMA (T_g = 71 °C), suggested a good moldability and higher compatibility of **1** with the current collector and the electrolyte solutions.

A large population of the cyclic nitroxide pendants in **1** produced a broad featureless ESR spectrum even in dilute solutions, as a result of a locally high density of the unpaired electrons. A CH_2Cl_2 solution of **1** showed a unimodal ESR signal at g = 2.0065 due to the spin exchange interaction between the unpaired electrons of the neighboring nitroxide group (Figure 3a, inset), in contrast to the spectrum obtained for a solution of the monomer **4** with the distinct hyperfine structure (Figure S1, inset). These spectra persisted without change for days at room temperature under air, which demonstrated the durability of the nitroxide radicals.

Electrode reaction of **1** in electrolyte solutions yielded a single voltammetric wave due to the nitroxide radical/oxoammonium cation couple with a magnitude of the current determined by the number of nitroxide groups present. The multiple, noninteracting redox behavior was based on the presence of many unpaired electrons each localized on different nitroxide groups, which gave rise to a paramagnetic response in a magnetization experiment. Static magnetic susceptibility of **1** was determined by SQUID measurements at 0.5 T and at various temperatures from 1.95 to 300 K. The resulting $\chi_{mol}T$ values at high temperatures corresponded to 0.375 emu K mol^{-1} calculated for a spin quantum number of $S = 1/2$, which supported the paramagnetic property (Figure 3a). The deviation of $\chi_{mol}T$ to lower values at low temperatures indicated a weak through-space antiferromagnetic interaction within the polymer.

The unpaired electron density in **1** was determined from the $1/\chi_{mol}$ vs T plots (Figure 3b), based on the Curie−Weiss rule according to $1/\chi_{para} = T/C - \theta/C$, where C is a Curie constant defined as $N_e g^2 \mu_B{}^2 S(S+1)/(3k_B)$. The slope of the $1/\chi_{mol}$ vs T plots corresponded to $1/C$ and gave an unpaired electron density of $N_e = 3.29 \times 10^{21}$ spin/g for **1**, which corresponded to 99.6% of the existing nitroxide groups in the polymer. The paramagnetic nature of **1** at room temperature also allowed determination of the unpaired electron density of ~99% by simply integrating the ESR signal and comparing the integrated magnitude with that of **4** as a standard, which roughly agreed with that from the SQUID measurement.

The spin-coating of a THF solution of **1** gave a uniform layer on an electrode surface. Contact stylus profile near a scratched edge gave a thickness of 180 nm under dry conditions and revealed a flat surface with a roughness of less than 4 nm. Cyclic voltammograms obtained for the layer revealed a reversible response at $(E_{pa} + E_{pc})/2 = 0.84$ V vs Ag/AgCl. The redox wave persisted

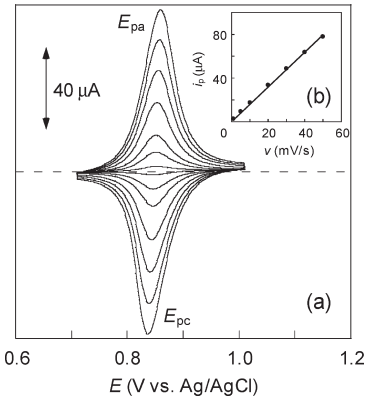

Figure 4. (a) Cyclic voltammograms for the layer of **1** at a scan rate of v = 1, 5, 10, 20, 30, 40, and 50 mV/s with the ascending order of peak currents (i_p). The electrolyte was a solution of 0.5 M $TBAClO_4$ in CH_3CN. The polymer layer was prepared on an ITO/glass plate. (b) Plots of i_p vs v showing the linearity.

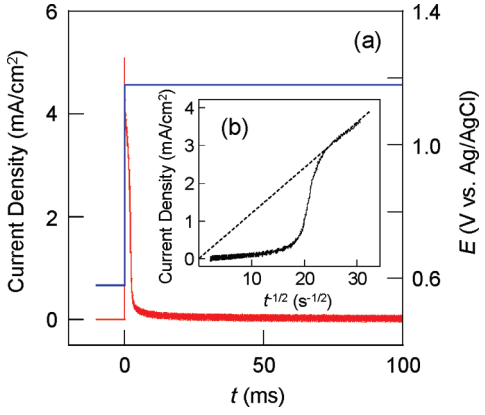

Figure 5. (a) $i-t$ curve for chronoamperometry (red curve) after applying a potential pulse of 0.6 to 1.2 V vs Ag/AgCl (blue line), obtained for the layer of **1**. The electrolyte was a solution of 0.5 M $TBAClO_4$ in CH_3CN. The polymer layer was prepared on an ITO/glass plate. (b) Cottrell plots for chronoamperometry. Dashed line corresponds to a semi-infinite diffusion process.

without change for several hours of continued charging/discharging cycling in CH_3CN, in which the dissolution of the layer was lower than the detection limits of the ESR spectroscopy (Figure 4a). The adhesive polyether layer stayed on electrodes without dissolution into the electrolyte solution. A monolayer-like redox behavior of the layer was demonstrated by the negligible peak-to-peak separation ΔE_p ($= E_{pa} - E_{pc}$), the peak current proportional to v in the range of 1−50 mV s^{-1} (Figure 4b), and the absence of the diffusion tail, which suggested that all redox sites in the layer, even not immediately adjacent to the electrode surface, were almost equilibrated with the electrode potential due to the rapid charge and counterion transport in the polymer layer (vide infra). Wave shapes with slightly larger ΔE_p of 13 mV at the scan rate of 50 mV/s suggested some contribution from the diffusion across the layer. The amount of charge consumed during the potential scan, determined by the integration of the voltammogram (146 mA h/g), coincided with the formula weight-based capacity of 147 mA h/g (Figure 1), which supported that all of the sites in the layer underwent the redox reaction.

Electroneutrality requires that the removal of each electron from the polymer layer result in the insertion of one ClO_4^- into the layer and/or the Donnan exclusion of the electrolyte cation. The dynamics of the propagating charge and ionic transport in the polymer layer gave insight into the nature of the processes responsible for the monolayer-like characteristics. The diffusion coefficient D for the propagating charge was determined from the Cottrell plots obtained from potential-step chronoamperometry which revealed the typical finite-diffusion behavior (Figure 5b). The slope of the Cottrell plot for the semi-infinite diffusion, which prevailed at the early stage of the electrolysis ($1 < t < 2$ ms), gave $D = 5.3 \times 10^{-11}$ cm^2/s. A relatively small degree of swelling allowed approximation of the redox site concentration of $C^* = 5.5$ M and a small intersite distance of $\delta_{av} = 6.7$ Å, based on the fw of **1** (Figure 1). Because the redox sites were immobilized in the polymer layer allowing only diffusional collision of the neighboring sites to undergo an electron self-exchange reaction, the charge propagation process involved an electron hopping mechanism with the bimolecular rate constant k_{ex} given by the Laviron−Andrieux−Savéant equation expressed by $D = k_{ex}\delta^2 C^*/6$, where δ was the center-to-center distance between the redox centers at the time of electron transfer[17] and was approximated by δ_{av} ($= (C^* N_A)^{-1/3}$).[17c] The electron self-exchange rate in the layer predicted from D was $k_{ex} = 1.4 \times 10^7$ M^{-1} s^{-1}, which was exceptionally large compared to those for the conventional redox polymers such as poly(vinylferrocene) (2×10^5 M^{-1} s^{-1})[18] and viologen-containing polymers (1.6×10^5 M^{-1} s^{-1})[19] and even larger than that for the TEMPO-substituted polynorbornene (1.8×10^5 M^{-1} s^{-1}) reported previously by our group.[9a] The rate constant in the polymer layer was almost comparable to that for nitroxides in homogeneous electrolyte solutions typically evaluated for the TEMPO/$TEMPO^+$ couple in CH_3CN and propylene carbonate ($k_{ex} \sim 10^8$ M^{-1} s^{-1}).[6c] The rapid electron exchange is most likely attributed to the small intersite distance as a result of the large population of the redox site to facilitate the electron hopping by orders of magnitude and the ionophoric polyether backbone to allow efficient counterion transport, which indicated that the charge propagation was dominated by the contribution from the electron hopping rather than that from the electrostatic attractive interaction of the ion pair.[17b]

The absence of substantial electric conductivity for **1** led us to examine their charge storage capability as a composite layer with a carbon nanofiber (VGCF) and a binder (PVdF). The polymer was coated on the surface of the carbon fiber by sufficient grinding of the mixture in NMP. The composite layer was placed on the surface of an electrode or a current collector by a solution-based wet process. A test cell was fabricated by sandwiching an electrolyte layer with the composite electrode and a Li foil using a separator film. The electrolyte was a conventional lithium salt, dissolved in ethylene carbonate/diethyl carbonate. The charging/discharging curves obtained for the fabricated cell at a constant current were characterized by the presence of a plateau voltage near 3.7 V (Figure 6), which was equal to the redox potential of **1** versus Li/Li^+. The charging process corresponded to the oxidation of the nitroxide radical to the oxoammonium cation at the cathode and the reduction of Li^+ to metallic Li at the anode. The cycle performance during the repeated charging−discharging process, recorded with cutoff voltages at 3.2 and 4.0 V, was free from significant deterioration in the charge-storage capability even after 400 cycles and persistent for 10^3 cycles (Figure 6).

A remarkable feature of the test cell with **1** is the capability of charging and discharging at large current densities of 10 C while maintaining the capacity and the plateau voltage (Figure 6). To characterize the rate performance, the test cell was charged at 10−120 C and then discharged at 10 C (Figure S2). The charging and discharging capacities gradually decreased with the C rate, probably as a result of the limitation from the Li anode. However, they were fairly well maintained even with the very rapid charging at 120 C, indicating that the test cell was fully charged in 30 s. The excellent rate capability, comparable to that of the supercapacitors, is attributed to the rapid charge and counterion transport in the layer of **1**. It may be noted that the plateau voltage,

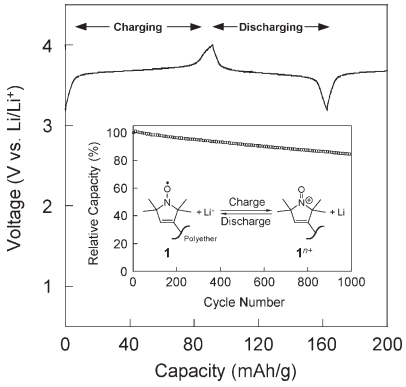

Figure 6. Charging and discharging curves for a coin cell at a current density of 10 C recorded between cutoff voltages at 3.2 and 4.0 V. The 1 C rate is defined as the current density at which the charging or discharging of the battery takes 1 h. The capacity of the cell was calculated per total weight of the loaded amount of **1**. The coin cell was fabricated with the **1**/carbon composite cathode and the Li anode sandwiching an electrolyte layer. The two electrodes were separated with a separator film (see Experimental Section for details). Inset: cycle performance of the cell.

inaccessible to the supercapacitors based on the double-layer charging, is accomplished by the Faradaic process of **1**, which is advantageous for high-density energy storage in batteries.

Preliminary experiments using an electrochemical quartz microbalance technique suggested that the amount of the electrolyte ions incorporated into or excluded from the layer of **1** for the charge neutralization was in agreement with the redox capacity determined by the coulometric measurements.[9a] The flexible and ionophoric polyether backbone in **1** allowed rapid electrode reaction of the nitroxide radicals and the efficient charge propagation within the polymer layer, which led to the excellent rate performances.

Our efforts have been directed toward tuning the redox potentials of the radical polymers to more negative side to use them as anode-active materials for an entirely organic radical battery.[8a] To be employed as the anode-active materials, the radical sites bound to the polyether backbones must undergo negative charging. Optimization of the radical sites and polyether backbones as well as the battery configuration is the topics of our continuous research.

Conclusion

The anionic coordinated ring-opening polymerization of the epoxide with the 2,2,5,5-tetramethyl-3-pyrrolin-1-oxyl group utilizing diethylzinc/H_2O as the initiator yielded the corresponding radical polyether, which was insoluble and yet swellable in electrolyte solutions by virtue of the high molecular weight. The unpaired electron in the monomer survived during the polymerization, giving rise to the large charge storage density. The radical polyether was characterized by the rapid charging and discharging capability, which was attributed to the efficient charge hopping throughout the polymer layer with the exceptionally large rate constant in the order of 10^7 M^{-1} s^{-1} due to the small intersite distance. The amorphous polyether backbone with a low glass transition temperature allowed efficient swelling in conventional electrolyte solutions, which enabled counterion transport for charge neutralization in the polymer layer. The organic-based rechargeable device fabricated with the polymer as the cathode-active material exhibited the high capacity and excellent charging−discharging properties. In particular, the cycle performance of the test cell persisted for 10^3 cycles with the high power-rate capability, which demonstrated the repeatability of the redox process of the nitroxide in the polymer.

Acknowledgment. This work was partially supported by Grants-in-Aid for Scientific Research (Nos. 19105003, 21550120, 21655043, and 21106519), the Global COE Program from MEXT, Japan, and the NEDO Project on "Radical Battery for Ubiquitous Power". We thank Dr. Shigeyuki Iwasa and Dr. Kentaro Nakahara of NEC Co. for technical discussions.

Supporting Information Available: Figures for the cyclic voltammogram and the ESR spectrum of **4** (Figure S1) and the rate performance of the test cell (Figure S2); tables for the results of polymerization of **4** and **8** (Table S1) and the crystallographic data on bond lengths, bond angles, and thermal displacement parameters for 3-carbamoyl-2,2,5,5-tetramethyl-3-pyrrolin-1-oxyl (Tables S2−S9) and 3-carbamoyl-2,2,5,5-tetramethyl-1-oxo-2,5-dihydro-1*H*-pyrrolium hexafluorophosphate (Tables S10−S17). This material is available free of charge via the Internet at http://pubs.acs.org.

References and Notes

(1) (a) Likhtenshtein, G. I.; Yamaguchi, J.; Nakatsuji, S.; Smirnov, A. I.; Tamura, R. *Nitroxides*; Wiley-VCH: Weinheim, 2008. (b) Hicks, R. G. *Org. Biomol. Chem.* **2007**, *5*, 1321–1338.

(2) (a) Oyaizu, K.; Nishide, H. *Adv. Mater.* **2009**, *21*, 2339–2344. (b) Yonekuta, Y.; Susuki, K.; Oyaizu, K.; Honda, K.; Nishide, H. *J. Am. Chem. Soc.* **2007**, *129*, 14128–14129. (c) Suga, T.; Takeuchi, S.; Ozaki, T.; Sakata, M.; Oyaizu, K.; Nishide, H. *Chem. Lett.* **2009**, *38*, 1160–1161.

(3) (a) Murata, H.; Miyajima, D.; Nishide, H. *Macromolecules* **2006**, *39*, 6331–6335. (b) Fukuzaki, E.; Nishide, H. *J. Am. Chem. Soc.* **2006**, *128*, 996–1001. (c) Fukuzaki, E.; Nishide, H. *Org. Lett.* **2006**, *8*, 1835–1838. (d) Kaneko, T.; Makino, T.; Miyaji, H.; Teraguchi, M.; Aoki, T.; Miyasaka, M.; Nishide, H. *J. Am. Chem. Soc.* **2003**, *125*, 3554–3557. (e) Michinobu, T.; Inui, J.; Nishide, H. *Org. Lett.* **2003**, *5*, 2165–2168. (f) Nishide, H.; Ozawa, T.; Miyasaka, H.; Tsuchida, E. *J. Am. Chem. Soc.* **2001**, *123*, 5942–5946. (g) Nishide, H.; Doi, R.; Oyaizu, K.; Tsuchida, E. *J. Org. Chem.* **2001**, *66*, 1680–1685. (h) Nishide, H.; Miyasaka, M.; Tsuchida, E. *Angew. Chem., Int. Ed.* **1998**, *37*, 2400–2402. (i) Takahashi, M.; Nishide, H.; Tsuchida, E.; Lahti, P. M. *Chem. Mater.* **1997**, *9*, 11–13. (j) Takahashi, M.; Tsuchida, E.; Nishide, H.; Yamada, S.; Matsuda, H.; Nakanishi, H. *Chem. Commun.* **1997**, 1853–1854. (k) Nishide, H.; Kaneko, T.; Igarashi, M.; Tsuchida, E.; Yoshioka, N.; Lahti, P. M. *Macromolecules* **1994**, *27*, 3082–3086. (l) Nishide, H.; Kaneko, T.; Yoshioka, N.; Akiyama, H.; Igarashi, M.; Tsuchida, E. *Macromolecules* **1993**, *26*, 4567–4571.

(4) (a) Pu, Y.-J.; Soma, M.; Kido, J.; Nishide, H. *Chem. Mater.* **2001**, *13*, 3817–3819. (b) Mukhopadhyay, S.; Topham, B. J.; Soos, Z. G.; Ramasesha, S. *J. Phys. Chem. A* **2008**, *112*, 7271–7279. (c) Namai, H.; Ikeda, H.; Hoshi, Y.; Kato, N.; Morishita, Y.; Mizuno, K. *J. Am. Chem. Soc.* **2007**, *129*, 9032–9036.

(5) (a) Sheldon, R. A.; Arends, I. W. C. E.; ten Brink, G.-J.; Dijksman, A. *Acc. Chem. Res.* **2002**, *35*, 774–781. (b) Osa, T.; Akiba, U.; Segawa, I.; Bobbitt, J. M. *Chem. Lett.* **1988**, 1423–1426. (c) Zhang, X.; Li, H.; Li, L.; Lu, G.; Zhang, S.; Gu, L.; Xia, Y.; Huang, X. *Polymer* **2008**, *49*, 3393–3398. (d) Allgaier, J.; Finkelmann, H. *Makromol. Chem., Rapid Commun.* **1993**, *14*, 267–271. (e) Miyazawa, T.; Endo, T.; Shiihashi, S.; Okawara, M. *J. Org. Chem.* **1985**, *50*, 1332–1334. (f) Semmelhack, M. F.; Chou, C. S.; Cortes, D. A. *J. Am. Chem. Soc.* **1983**, *105*, 4492–4494. (g) Suguro, M.; Mori, A.; Iwasa, S.; Nakahara, K.; Nakano, K. *Macromol. Chem. Phys.* **2009**, *210*, 1402–1407.

(6) (a) Suga, T.; Pu, Y.-J.; Oyaizu, K.; Nishide, H. *Bull. Chem. Soc. Jpn.* **2004**, *77*, 2203–2204. (b) Yonekuta, Y.; Oyaizu, K.; Nishide, H. *Chem. Lett.* **2007**, *36*, 866–867. (c) Grampp, G.; Rasmussen, K. *Phys. Chem. Chem. Phys.* **2002**, *4*, 5546–5549. (d) Buhrmester, C.; Moshurchak, L. M.; Wang, R. L.; Dahn, J. R. *J. Electrochem. Soc.* **2006**, *153*, A1800–A1804. (e) Nakahara, K.; Iwasa, S.; Iriyama, J.; Morioka, Y.; Suguro, M.; Satoh, M.; Cairns, E. J. *Electrochim. Acta* **2006**, *52*, 921–927.

(7) (a) Nishide, H.; Oyaizu, K. *Science* **2008**, *319*, 737–738. (b) Novák, P.; Müller, K.; Santhanam, K. S. V.; Haas, O. *Chem. Rev.* **1997**, *97*, 207–281. (c) Coppo, P.; Turner, M. L. *J. Mater. Chem.* **2005**, *15*, 1123–1133. (d) Roncali, J. *J. Mater. Chem.* **1997**, *7*, 2307–2321. (e) Nishide, H.; Suga, T. *Electrochem. Soc. Interface* **2005**, *14* (4), 32–36. (f) Oyaizu, K.; Hatemata, A.; Choi, W.; Nishide, H. *J. Mater. Chem.* **2010**, *20*, 5404–5410.

(8) (a) Suga, T.; Ohshiro, H.; Sugita, S.; Oyaizu, K.; Nishide, H. *Adv. Mater.* **2009**, *21*, 1627–1630. (b) Suga, T.; Konishi, H.; Nishide, H. *Chem. Commun.* **2007**, 1730–1732. (c) Suga, T.; Pu, Y.-J.; Kasatori, S.; Nishide, H. *Macromolecules* **2007**, *40*, 3167–3173. (d) Takahashi, Y.; Hayashi, N.; Oyaizu, K.; Honda, K.; Nishide, H. *Polym. J.* **2008**, *40*, 763–767.

(9) (a) Oyaizu, K.; Ando, Y.; Konishi, H.; Nishide, H. *J. Am. Chem. Soc.* **2008**, *130*, 14459–14461. (b) Koshika, K.; Sano, N.; Oyaizu, K.; Nishide, H. *Chem. Commun.* **2009**, 836–838.

(10) (a) Nishide, H.; Iwasa, S.; Pu, Y.-J.; Suga, T.; Nakahara, K.; Satoh, M. *Electrochim. Acta* **2004**, *50*, 827–831. (b) Bugnon, L.; Morton, C. J. H.; Novak, P.; Vetter, J.; Nesvadba, P. *Chem. Mater.* **2007**, *19*, 2910–2914. (c) Kim, J.-K.; Cheruvally, G.; Choi, J.-W.; Ahn, J.-H.; Choi, D. S.; Song, C. E. *J. Electrochem. Soc.* **2007**, *154*, A839–A843. (d) Nakahara, K.; Iriyama, J.; Iwasa, S.; Suguro, M.; Satoh, M.; Cairns, E. J. *J. Power Sources* **2007**, *163*, 1110–1113. (e) Nakahara, K.; Iriyama, J.; Iwasa, S.; Suguro, M.; Satoh, M.; Cairns, E. J. *J. Power Sources* **2007**, *165*, 398–402. (f) Nakahara, K.; Iriyama, J.; Iwasa, S.; Suguro, M.; Satoh, M.; Cairns, E. J. *J. Power Sources* **2007**, *165*, 870–873. (g) Nakahara, K.; Iwasa, S.; Satoh, M.; Morioka, Y.; Iriyama, J.; Suguro, M.; Hasegawa, E. *Chem. Phys. Lett.* **2002**, *359*, 351–354. (h) Yoshihara, S.; Isozumi, H.; Kasai, M.; Yonehara, H.; Ando, Y.; Oyaizu, K.; Nishide, H. *J. Phys. Chem. B* **2010**, *114*, 8335–8340.

(11) (a) Koshika, K.; Sano, N.; Oyaizu, K.; Nishide, H. *Macromol. Chem. Phys.* **2009**, *210*, 1989–1995. (b) Suguro, M.; Iwasa, S.; Nakahara, K. *Electrochem. Solid-State Lett.* **2009**, *12*, A194–A197. (c) Suguro, M.; Iwasa, S.; Nakahara, K. *Macromol. Rapid Commun.* **2008**, *29*, 1635–1639. (d) Suguro, M.; Iwasa, S.; Kusachi, Y.; Morioka, Y.; Nakahara, K. *Macromol. Rapid Commun.* **2007**, *28*, 1929–1933.

(12) (a) Oyaizu, K.; Suga, T.; Yoshimura, K.; Nishide, H. *Macromolecules* **2008**, *41*, 6646–6652. (b) Suga, T.; Yoshimura, K.; Nishide, H. *Macromol. Symp.* **2006**, *245*−*246*, 416–422. (c) Endo, T.; Takuma, K.; Takata, T.; Hirose, C. *Macromolecules* **1993**, *26*, 3227–3229.

(13) (a) Bard, A. J.; Faulkner, L. R. *Electrochemical Methods, Fundamentals and Applications*, 2nd ed.; Wiley: New York, 2001. (b) Nicholson, R. S. *Anal. Chem.* **1965**, *37*, 1351–1355.

(14) (a) Corey, E. J.; Chaykovsky, M. *J. Am. Chem. Soc.* **1965**, *87*, 1353–1364. (b) Corey, E. J.; Oppolzer, W. *J. Am. Chem. Soc.* **1964**, *86*, 1899–1900.

(15) Winter, M.; Brodd, R. J. *Chem. Rev.* **2004**, *104*, 4245–4269.

(16) Kanoh, S.; Takemura, A.; Fukuda, K.; Chinwanitcharoen, C.; Motoi, M. *J. Polym. Sci., Polym. Chem. Ed.* **2004**, *42*, 4570–4579.

(17) (a) *Molecular Design of Electrode Surfaces*; Murray, R. W., Ed.; Wiley-Interscience: New York, 1992. (b) Bu, H.; English, A. M.; Mikkelsen, S. R. *J. Phys. Chem. B* **1997**, *101*, 9593–9599. (c) Sosnoff, C. S.; Sullivan, M.; Murray, R. W. *J. Phys. Chem.* **1994**, *98*, 13643–13650.

(18) Sullivan, M. G.; Murray, R. W. *J. Phys. Chem.* **1994**, *98*, 4343–4351.

(19) Dalton, E. F.; Murray, R. W. *J. Phys. Chem.* **1991**, *95*, 6383–6389.